Supplementary Material

Rare earth-Mediated Synergistic Lattice Stabilization and Interface Protection for Suppressed Phase Transition and Superior Electrochemical Performance in Ni-Rich Cathodes

Experimental Section

Synthesis Procedures*:* The $Ni_{0.83}Co_{0.11}Mn_{0.06}(OH)_2$ precursor was thoroughly mixed with $LiOH{\cdot}H_2O$ in a molar ratio of 1:1.05 using an agate mortar. Subsequently, the mixture underwent calcination first at 500 ◦C for 6 h and then at 780 ◦C for 12 h under an O_2 atmosphere to yield $LiNi_{0.83}Co_{0.11}Mn_{0.06}O_2$. For clarity in comparison, the resulting $LiNi_{0.83}Co_{0.11}Mn_{0.06}O_2$ was designated as NCM-0 in this work. Samarium nitrate hexahydrate and NCM-0 were added to a beaker filled with deionized water, where the molar ratio of samarium nitrate hexahydrate to NCM-0 was 1:100. After stirring for 30 minutes, the mixture was subjected to spray drying to obtain dry powder.

Subsequently, the powder was placed in a tube furnace and annealed at 700° C for 4 hours under an oxygen atmosphere, yielding NCM-2. For comparison, the NCM-1 and NCM-3 materials were synthesized by the similar method. The difference lies in that the molar ratios of samarium nitrate hexahydrate to NCM-0 are 0.5:100 and 2:100 respectively.

Material Characterizations: The XRD patterns of as-investigated materials, both in their pristine state and after modification, were examined using a Bruker D8 Advance X-ray diffractometer equipped with a Cu-target Kα radiation source. The measurements were performed over a scanning range of 10° to 90° at a scanning speed of 2° per minute. The phases were identified using HighScore Plus software. The lattice constants and ionic occupancy ratios were determined through Rietveld refinement using the FullProf suite. The morphology of the cathode particles and the surface morphology of the cathode foil after cycling were analyzed using a scanning electron microscope (SU3800) from Hitachi. The microstructures and elemental distributions within the samples were investigated using a transmission electron microscope (JEM-2010F and Talos F200S). An X-ray photoelectron spectrometer (Nexsa) was utilized to characterize the surface and near-surface regions of the materials, as well as the surface of the foil after cycling, to obtain relevant information.

Electrochemical Test: To fabricate the cathode material, 0.4 g of the synthesized cathode materials, 0.05 g of acetylene black, and 0.05 g of polyvinylidene fluoride (PVDF) were measured out in a mass ratio of 8:1:1 and thoroughly blended. The blend was subsequently transferred to a weighing bottle, and 1 mL of N-methylpyrrolidone (NMP) was introduced. The mixture was magnetically agitated for 2 hours to achieve a uniform slurry. This slurry was uniformly applied onto an aluminum foil substrate and dried in a vacuum oven at 80 °C for 2 hours. Thereafter, the coated foil was compressed at a pressure of 1.0×10^7 Pa using a pressing machine. The compressed foil was then dried once more in a vacuum oven at 80 °C for 24 hours and stored in an inert atmosphere glove box for subsequent use.
The electrochemical evaluations were performed using 2032-type coin half-cells, which were assembled with lithium metal serving as the anode, Celgard 2500 as the separator, and an electrolyte consisting of 1 M $LiPF_6$ dissolved in a mixture of dimethyl carbonate (DMC), diethyl carbonate (DEC), and ethylene carbonate (EC) in a 1:1:1 volume ratio. The electrochemical performances, such as the initial coulombic efficiency, discharge specific capacity, cycle retention rate, and rate capability, were assessed via constant-current charge/discharge tests within a voltage window of 2.8-4.5 V at an ambient temperature of around 25 °C. During the cycling evaluations, the cells were initially discharged at a rate of 0.2C for the first five cycles, subsequently proceeding to a 1C discharge rate for the ensuing 100 cycles. The rate capability assessment commenced with an initial charge at 0.2C, succeeded by sequential discharges escalating from 0.2C to 10C, and culminating in a return to the 0.2C discharge rate. The galvanostatic intermittent titration technique (GITT) was executed with a current density of 0.2C, entailing 10 minutes of constant current charge/discharge succeeded by a 40-minute relaxation interval. Cyclic voltammetry (CV) examinations were conducted utilizing a Bio-Logic SP150e electrochemical workstation, with potential scans spanning from 2.8 to 4.5 V at a scan velocity of 0.2 mV/s. The alternating current impedance spectroscopy (EIS) measurements were performed across an AC frequency spectrum of 100 kHz to 0.01 Hz, employing an AC amplitude of 5 mV.

Density functional theory (DFT) calculation: All the computations were carried out by spin-polarized DFT method, as implemented in Vienna ab initio Simulation Package (VASP)[S1,S2]. The exchange correlation energy was modeled by the Perdew−Burke−Ernzerhof (PBE) functional within the generalized gradient approximation (GGA)[S3]. An energy cutoff of 450 eV was adopted for the plane-wave basis. In structural optimizations, the energy and force convergence thresholds were set to 10^{-5} eV and 0.05 eV/Å, respectively. A 2 × 2 × 1 supercell model with hexagonal structure was constructed for $LiNiO_2$ unit cell to optimize its lattice geometry. The Brillouin zone was sampled by 5 × 5 × 2 k-points using the Monkhorst−Pack scheme. The climbing-image nudged elastic band (CI-NEB) method[S4] was utilized to obtain the kinetic barriers. Visualization of the results was performed using VESTA[S5], and postprocessing of the VASP data was carried out using VASPKIT[S6].

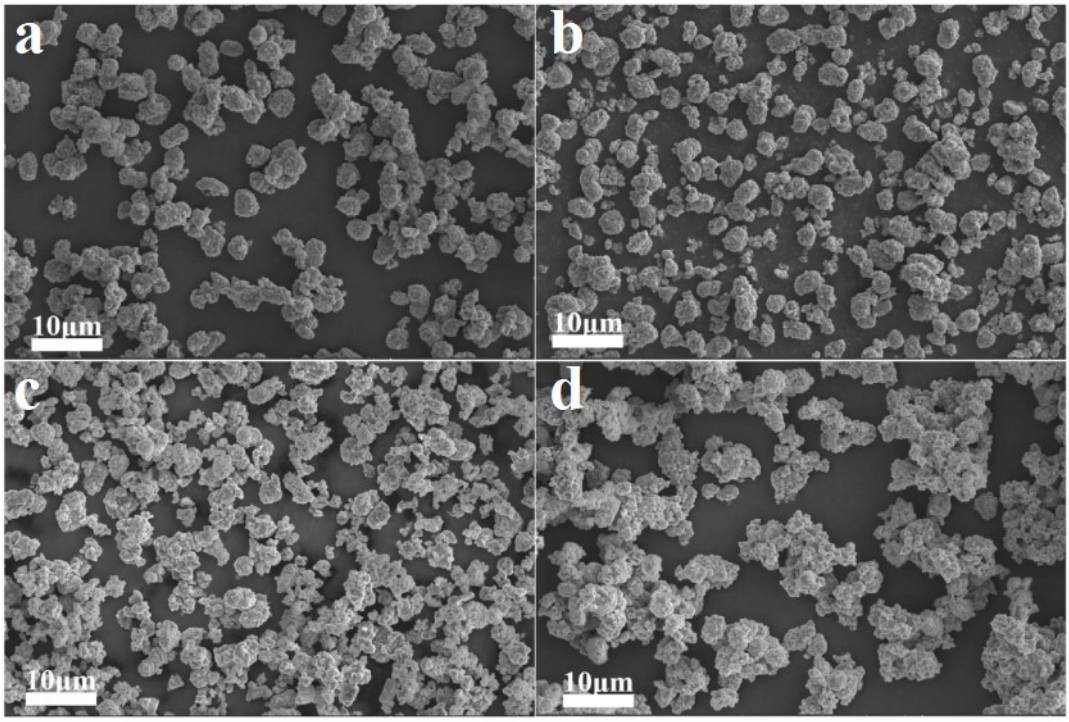

Fig. S1 SEM of NCM-0 (a), NCM-1 (b), NCM-2 (c) and NCM-3 (d).

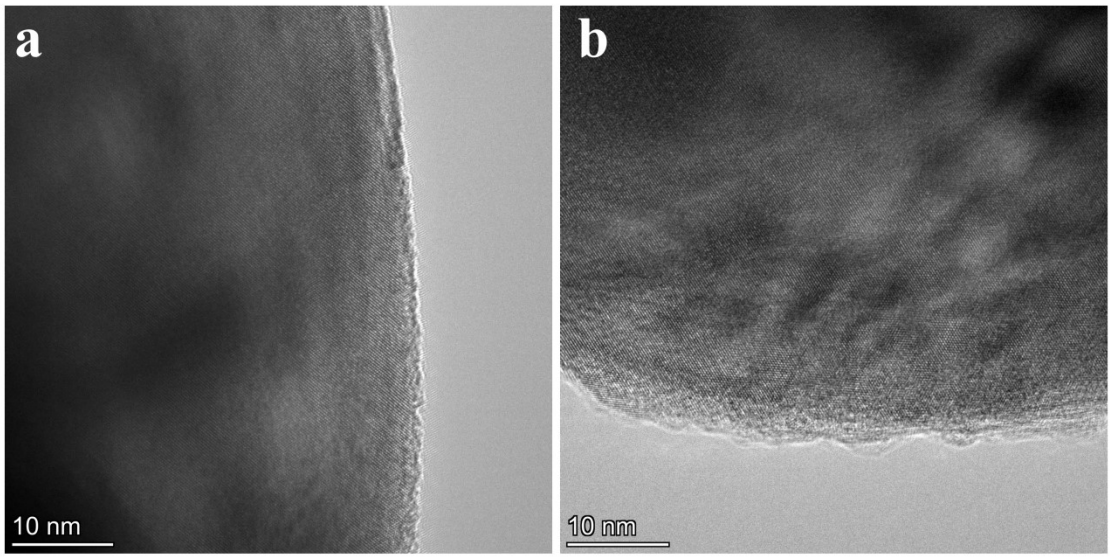

Fig. S2 HR-TEM images of (a) NCM-1, (b) NCM-3

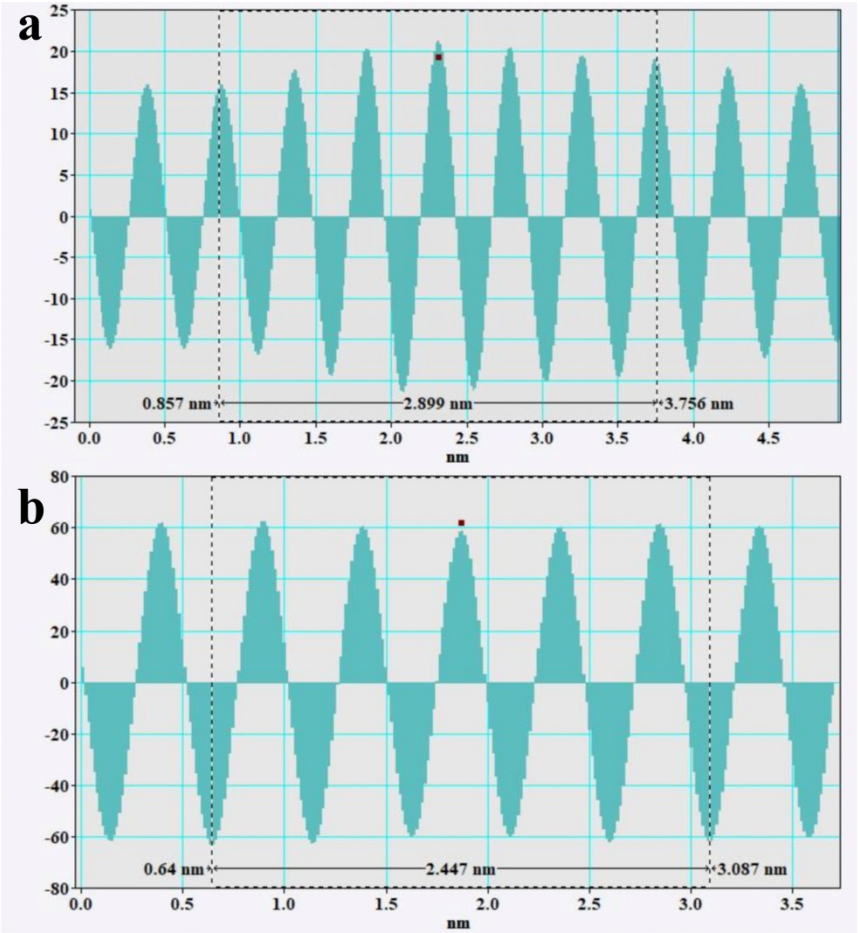

Fig. S3 FFT patterns of (a) NCM-0, (b) NCM-2

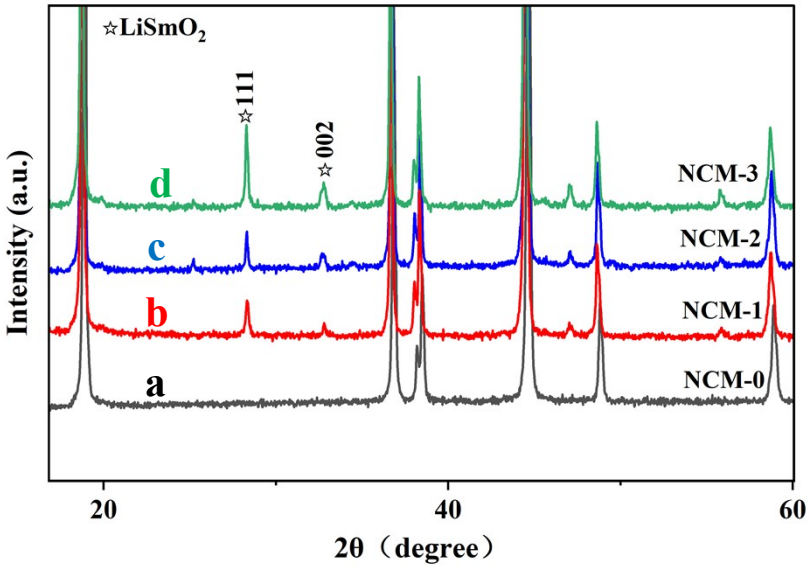

Fig. S4 XRD patterns of NCM-0 (a), NCM-1 (b), NCM-2 (c) and NCM-3 (d).

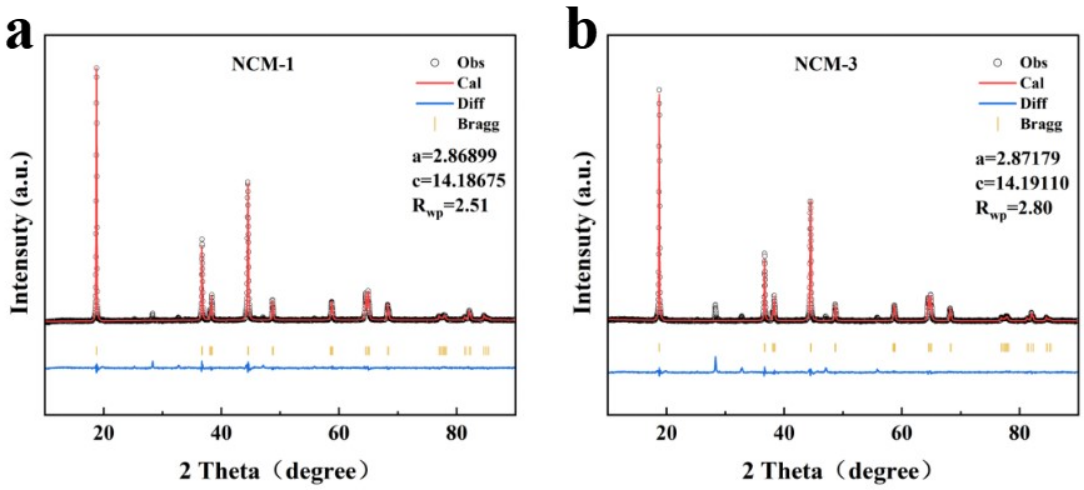

Fig. S5 Rietveld refinement patterns of NCM-0 (a) and NCM-3 (b).

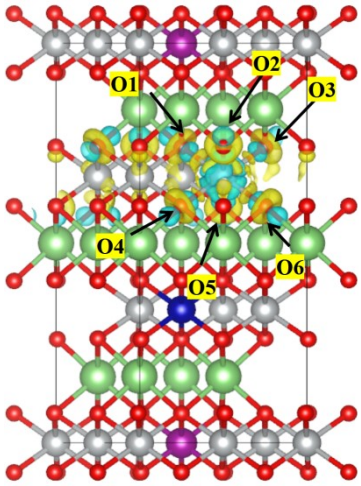

Fig. S6 VCDD of NCM-0.

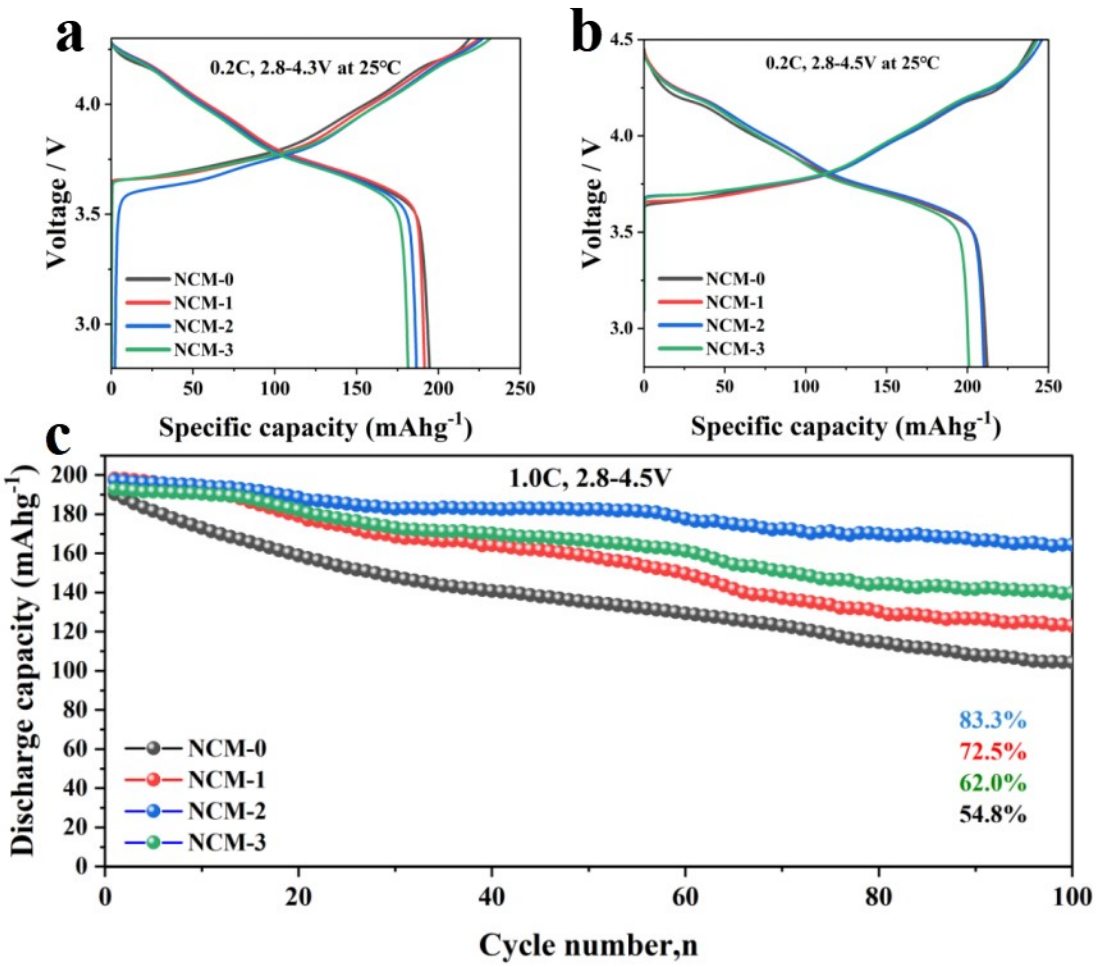

Fig. S7 First charge/discharge curves at 0.2C within the voltage range 2.8-4.3 V (a) , 2.8-4.5 V (b) and the cyclic performance (c) in the voltage range of 2.8-4.5 V.

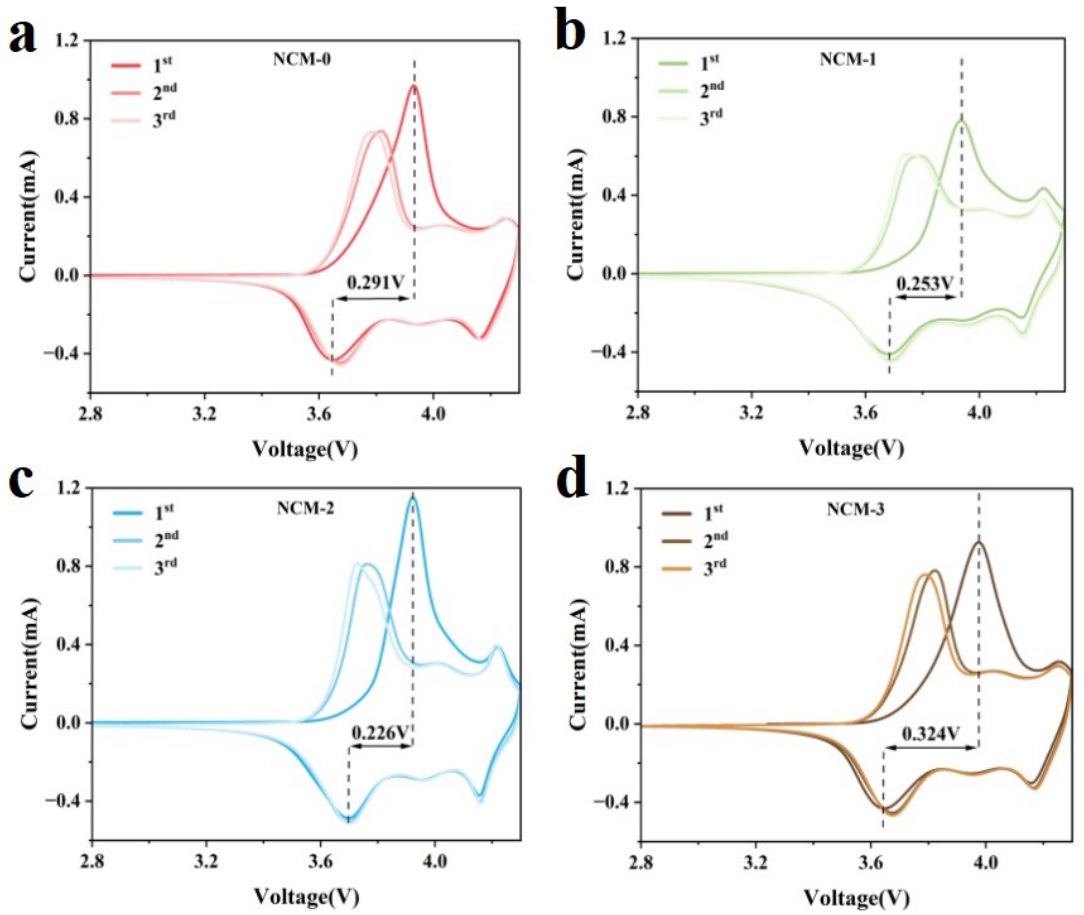

Fig. S8 Cyclic voltammetry curves (CV) of NCM-0 (a), NCM-1 (b), NCM-2 (c) and NCM-3 (d) at different scan rates.

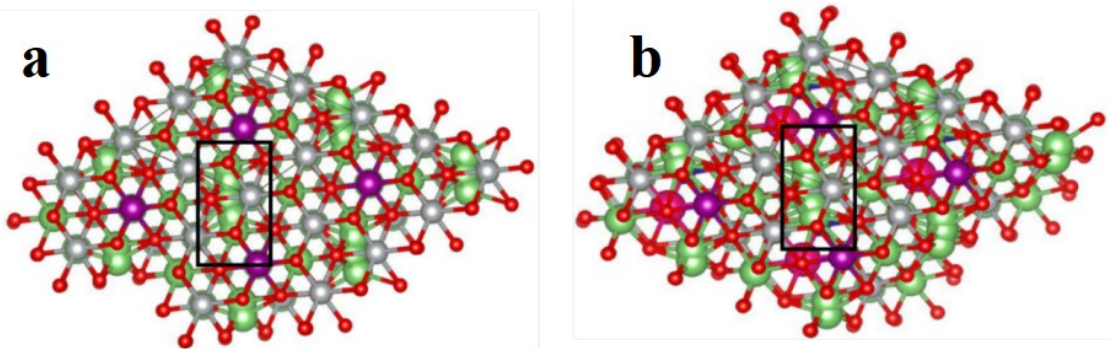

Fig. S9 Diffusion path of lithium-ion of NCM-0 (a) and NCM-2 (b);

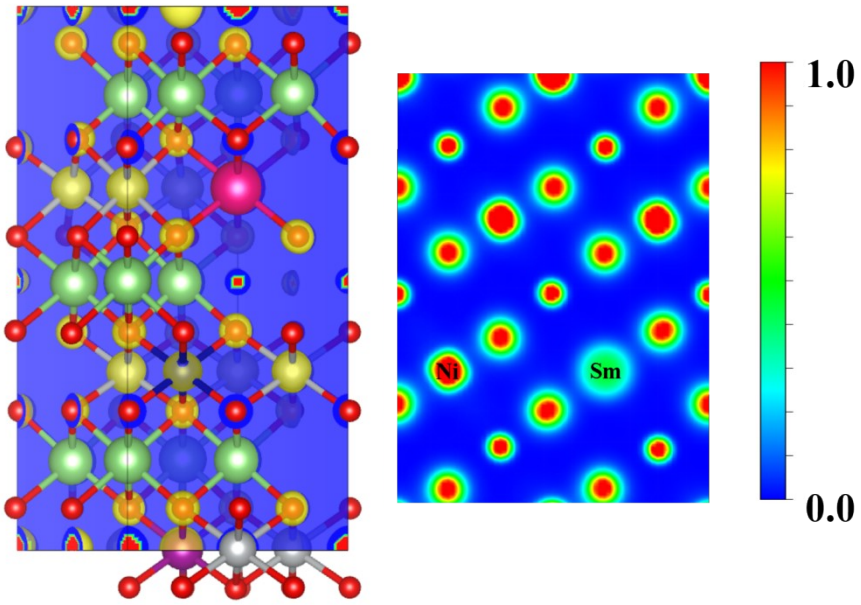

Fig. S10 2D charge density distribution.

Table S1 Lattice parameters of the NCM-0, NCM-1, NCM-2 and NCM-3calculated from X-ray Rietveld refinement.

Samples	a[Å]	c[Å]	c/a	I(003)/I(104)	Li^{+}/Ni^{2+} mixing	Rwp[%]	χ^2
NCM-0	2.86988	14.18513	4.9428	2.0532	2.75	2.81	1.16
NCM-1	2.86899	14.18675	4.9448	2.0527	2.83	2.51	1.74
NCM-2	2.87264	14.19415	4.9411	2.0534	2.51	2.30	1.60
NCM-3	2.87179	14.19110	4.9415	2.0529	2.81	2.80	2.16

Table S2 Impedance data from Nyquist plots for NCM-0 and NCM-2 before and after cycling.

Samples	Before test		After 150 cycles		
	Rs	Rct	Rs	Rf	Rct
NCM-0	6.26	45.29	78.56	293.5	1142.4
NCM-2	10.78	69.82	63.31	226.7	530.8

Table S3 The detailed initial charge-discharge data of all samples at 0.2C within the voltage range 2.8-4.3 V.

Samples	Initial charge capacity (mAh g^{-1})	Initial discharge capacity (mAh g^{-1})	Initial coulombic efficiency (%)
NCM-0	219.12	194.48	88.75
NCM-1	224.99	191.43	85.08
NCM-2	227.39	186.54	82.03
NCM-3	231.97	181.38	78.19

Table S4 The detailed initial charge-discharge data of all samples at 0.2C within the voltage range 2.8-4.5 V.

Samples	Initial charge capacity (mAh g-1)	Initial discharge capacity (mAh g-1)	Initial coulombic efficiency (%)
NCM-0	241.44	212.33	87.94
NCM-1	246.13	210.50	85.53
NCM-2	245.90	210.15	85.46
NCM-3	243.18	200.85	82.59

Table S5 Elemental content of Sm in different samples after ICP-MS testing.

Samples	m_0（g）	V_0（mL）	Test element	C_o（ug/L）	f	C_1（ug/L）	C_x（ug/kg）	W（%）
NCM-2	0.0527	25	Sm	238.6003	100	23860.0270	11318798.3871	1.1319%
NCM-2	0.0527	25	Sm	243.1229	100	24312.2940	11533346.2998	1.1533%
NCM-2	0.0527	25	Sm	244.1447	100	24414.4690	11581816.4137	1.1582%
NCM-3	0.0509	25	Sm	57.7748	1000	57774.7500	28376596.2672	2.8377%
NCM-3	0.0509	25	Sm	60.0395	1000	60039.4800	29488939.0963	2.9489%
NCM-3	0.0509	25	Sm	60.1970	1000	60196.9900	29566301.5717	2.9566%

Table S6 Comparison of the cycle stability of NCM-2 with the nickel-rich cathode materials as reported elsewhere, as the cathode materials for coin half cells.

Sample	Charge/Discharge current rate ($mA\ g^{-1}$)	Voltage range (V)	Initial capacity ($mAhg^{-1}$)	Capacity after cycling ($mAhg^{-1}$)	Capacity retention/cycles	Ref.
NCM-2	**200/200**	**2.8-4.3**	**186.5**	**176.2**	**94.5%/150**	**This work**
NCM-2	**200/200**	**2.8-4.5**	**210.2**	**175.1**	**83.3%/100**	**This work**
TBO7-SC-NCM	200/200	2.7-4.3	224.6	193.7	95.4%/100	[S7]
SC-NCM-AS	200/200	2.75-4.4	222.4	179.3	86.2%/100	[S8]
Z/T@SC-NCM-0.2	0.3C/0.3C	2.75-4.6	180.0	159.3	88.5%/150	[S9]
Z2-NCM@B2	170/170	2.95-4.3	145.0	138.8	95.7%/200	[S10]
AZO3-SNCM	100/100	2.75-4.3	193	180	93.3%/150	[S11]
B-NCM	1C/1C	3.0-4.5	193.5	169.1	87.4%/150	[S12]
SNCM@Nb-2	200/200	2.7-4.3	197.2	182.4	92.5%/100	[S13]
Ta-NCM811	100/100	3.0-4.3	186.0	168.1	90.4%/200	[S14]

Reference

[S1] Hafner, Jürgen. "Ab-initio simulations of materials using VASP: Density-functional theory and beyond." Journal of computational chemistry 29.13 (2008): 2044-2078, https://doi.org/10.1002/jcc.21057.

[S2] Blöchl, Peter E. "Projector augmented-wave method." Physical review B 50.24 (1994): 17953, https://doi.org/10.1103/PhysRevB.50.17953.

[S3] Perdew, John P., Kieron Burke, and Matthias Ernzerhof. "Generalized gradient approximation made simple." Physical review letters 77.18 (1996): 3865,

https://doi.org/10.1103/PhysRevLett.77.3865.
[S4] Henkelman, Graeme, Blas P. Uberuaga, and Hannes Jónsson. "A climbing image nudged elastic band method for finding saddle points and minimum energy paths." The Journal of chemical physics 113.22 (2000): 9901-9904, https://doi.org/10.1063/1.1329672.
[S5] Momma, Koichi, and Fujio Izumi. "VESTA 3 for three-dimensional visualization of crystal, volumetric and morphology data." Applied Crystallography 44.6 (2011): 1272-1276, https://doi.org/10.1107/S0021889811038970.
[S6] Wang, Vei, et al. "VASPKIT: A user-friendly interface facilitating high-throughput computing and analysis using VASP code." Computer Physics Communications 267 (2021): 108033, https://doi.org/10.1016/j.cpc.2021.108033.
[S7] Zeng, Chenrui, et al. "Phase compatible surface engineering to boost the cycling stability of single-crystalline Ni-rich cathode for high energy density lithium-ion batteries." Energy Storage Materials 72 (2024): 103788, https://doi.org/10.1016/j.ensm.2024.103788.
[S8] Li, Jing, et al. "Mechanistic origin for high structural stability of single crystalline nickel-rich cathode materials via Al and Sm co-doping." Advanced Functional Materials 33.24 (2023): 2300127, https://doi.org/10.1002/adfm.202300127.
[S9] Zhang, Zhi, et al. "In situ co-doping strategy for achieving long-term cycle stability of single-crystal Ni-rich cathodes at high voltage." Chemical Engineering Journal 445 (2022): 136825, https://doi.org/10.1016/j.cej.2022.136825.
[S10] Shen, Jixue, et al. "Realizing ultrahigh-voltage performance of single-crystalline LiNi0. 55Co0. 15Mn0. 3O2 cathode materials by simultaneous Zr-doping and B2O3-coating." Journal of Alloys and Compounds 903 (2022): 163999, https://doi.org/10.1016/j.jallcom.2022.163999.
[S11] Ou, Xing, et al. "Enabling high energy lithium metal batteries via single-crystal Ni-rich cathode material co-doping strategy." Nature communications 13.1 (2022): 2319, https://doi.org/10.1038/s41467-022-30020-4.
[S12] Li, Minghuang, et al. "The effect of B2O3/Li3BO3 coating and B3+ doping on electrochemical properties in nickel-rich single-crystal LiNi0. 7Co0. 2Mn0. 1O2 cathodes." Journal of Alloys and Compounds 907 (2022): 164489, https://doi.org/10.1016/j.jallcom.2022.164489.
[S13] Jamil, Sidra, et al. "Significantly fastened redox kinetics in single crystal layered oxide cathode by gradient doping." Nano energy 94 (2022): 106961, https://doi.org/10.1016/j.nanoen.2022.106961.
[S14] Zou, Yu-Gang, et al. "Mitigating the kinetic hindrance of single-crystalline Ni-Rich cathode via surface gradient penetration of tantalum." Angewandte Chemie International Edition 60.51 (2021): 26535-26539, https://doi.org/10.1002/anie.202111954.